



## OPEN Climate change and variability drive increasing exposure of marine heatwaves across US estuaries

Ricardo U. Nardi<sup>1</sup>✉, Piero L. F. Mazzini<sup>1</sup> & Ryan K. Walter<sup>2</sup>

Marine heatwaves (MHWs) are among the greatest threats to marine ecosystems, and while substantial advances have been made in oceanic MHWs, little is known about estuarine MHWs. Utilizing a temperature dataset spanning over two decades and 54 stations distributed across 20 estuaries in the United States National Estuarine Research Reserve System, we present a comprehensive analysis of estuarine MHW characteristics and trends. Long-term climate-change-driven warming is driving more frequent MHWs along the East Coast, and if trends continue, this region will be in a MHW state for ~1/3 of the year by the end of the century. In contrast, the vast majority of the West Coast showed no trends, highlighting the potential for future thermal refugia. The West Coast was more strongly influenced by climate variability through the enhancement/suppression of MHWs during different phases of climate modes, suggesting long-term predictability potential. These results can provide guidance for management actions and planning in these critical environments.

Marine Heatwaves (MHWs)—prolonged periods of anomalously warm seawater temperature<sup>1</sup>—have emerged as one of the greatest threats to marine biodiversity amid a warming planet. These extreme temperature events can cause long lasting detrimental effects to marine ecosystems including mass mortalities, habitat loss and compression, species migration, and increased ocean stressors such as low pH and dissolved oxygen<sup>2–5</sup>. They also critically disrupt essential ecosystem services<sup>6–12</sup> and can destabilize socioeconomic systems by collapsing fisheries and aquaculture, thereby threatening food security and impacting human society<sup>2–4,13</sup>.

Over the past few decades, the frequency, intensity, and duration of MHWs have been increasing globally<sup>14,15</sup>. These trends are expected to persist throughout the twenty-first century, with projections suggesting that much of the open ocean could reach a near-permanent MHW state by the late century<sup>3</sup>. These trends have been attributed to both rising mean sea surface temperature (SST) and increasing SST variability<sup>16,17</sup>. Although increasing mean temperature and variance both influence MHW patterns worldwide, long-term SST trends associated with anthropogenic climate change is recognized as the primary driver behind the ongoing increase in MHWs<sup>14,16,18–20</sup>, surpassing the effects of increasing variance, or internal variability<sup>16,21,22</sup>.

While climate change drives long-term trends in MHWs, climate variability is known to modulate their frequency and intensity on shorter timescales<sup>23–26</sup>. This modulation is connected to large-scale climate modes of variability (e.g., El Niño–Southern Oscillation - ENSO), which can either enhance or suppress MHWs by directly modifying ocean temperatures and through teleconnections (e.g., atmospheric bridge, planetary waves) that link distant climate forcing with regional impacts<sup>23,24</sup>. These remotely induced fluctuations can trigger oceanic disturbances that travel vast distances via Rossby and Kelvin waves, redistributing heat and modulating local heat budgets, resulting in distinct regional patterns of MHW variability observed worldwide<sup>17,23,27,28</sup>.

Although the drivers and dynamics of MHWs in the broader global ocean are well-established<sup>15,17,23,29–39</sup>, their behavior in estuarine systems remains relatively unknown. Estuaries are among the most productive, but also threatened, ecosystems in the world, supporting a rich diversity of economically- and ecologically-important species, many ecosystem services, and vital economic activities<sup>40</sup>. However, recent research demonstrates that these systems have been severely impacted by MHW events, leading to major fish kills<sup>41</sup>, deoxygenation and biodiversity loss<sup>42</sup>, long-lasting declines in macroalgae biomass<sup>43,44</sup>, and shifts in seagrass dominance and carbon stocks<sup>45,46</sup>. Furthermore, MHWs can lead to multi-stressor compound events such as low dissolved oxygen and pH levels<sup>47</sup>, as well as the expansion of hypoxic zones during MHW events<sup>48</sup>.

The lack of understanding of MHWs in estuarine systems can largely be attributed to the challenges in observing water temperature at a sufficient temporal resolution (at least daily) and maintaining the long-term records, on the order of decades, necessary to accurately characterize these events<sup>37,47,49</sup>. While satellite data are effective for broader oceanic and continental shelf studies, they often fail to accurately resolve nearshore and

<sup>1</sup>Virginia Institute of Marine Science, William & Mary, Gloucester Point, VA, USA. <sup>2</sup>Physics Department, California Polytechnic State University, San Luis Obispo, CA, USA. ✉email: rutzignardi@vims.edu

estuarine environments due to their complex shorelines and smaller spatial scales<sup>36,37,49</sup>. As a result, research using continuous, long-term in-situ data to explore the physical mechanisms behind MHWs in estuaries has been limited, despite the major ecosystem implications<sup>36,48,49</sup>. Recent research found that in Chesapeake Bay, the largest estuary in the United States, both climate change and variability played a key role in the dynamics of MHWs<sup>49</sup>. In addition to documenting increases in MHW frequency primarily driven by long-term warming resulting from anthropogenic climate change, similar to trends observed in the global ocean, they also found significant changes in the likelihood of MHW occurrence in response to different phases of climate modes of variability<sup>14,15,49</sup>. There is a critical and urgent need to evaluate how MHWs in other estuarine systems respond to climate change and variability, with important implications for ecosystem resilience amid a warming planet.

Here, we take advantage of a unique system of long-term monitoring platforms across the United States as part of the National Estuarine Research Reserve System (NERRS) and provide the most extensive assessment of MHWs in estuaries and the impact of climate change and variability on these extreme temperature events. This novel dataset includes high-frequency in-situ near surface temperature measurements spanning more than two decades from 54 stations across 20 estuaries (Fig. 1), covering a vast spatial domain with a wide range of geographic features and climates. This study focuses on characterizing MHWs; investigating their trends, spatial co-occurrence, and the relative contribution of long-term temperature increases versus temperature variance driving MHW trends; and assessing the influence of large-scale climate modes on MHW occurrences. We find that East Coast estuaries are highly vulnerable to climate change, while West Coast estuaries may serve as future “thermal refugia” for MHWs. Additionally, a strong link between large-scale climate modes and MHW occurrences, especially on the West Coast, highlights the potential for long-term MHW forecasting, offering critical insights for future climate adaptation and enhancing estuarine resilience.

## Results

### MHW events

MHW metrics across all sites exhibited pronounced spatial variability (Fig. 2). Mean intensity, cumulative intensity, and yearly cumulative intensity were statistically significant different between the East and West Coasts of the U.S. at the 95% confidence level, with the East Coast generally showing higher values (Fig. 2c, e, f). Across all sites, the average annual frequency of MHW events (Fig. 2a) was 2.23 events per year. The highest average frequency was observed at Elkhorn Slough, CA, with 3.03 events per year, while the lowest frequency occurred at Kachemak Bay, AK, with 1.55 events per year. Despite having the lowest frequency of MHW events, Kachemak Bay, AK recorded the longest average duration, with events lasting 22.34 days Fig. (2b), notably exceeding all other sites. Across all estuaries, the average MHW duration was 8.3 days, with the shortest duration observed in Chesapeake Bay, MD, at 6.41 days. Across all sites, the annual average number of MHW days Fig. (2d) was 18.70 days per year. Kachemak Bay, AK, recorded the highest number of average MHW days, with 30.65 days per year, while North Carolina, NC, had the fewest, at 11.18 days per year.

Overall, the mean intensity across all estuaries was 3.13 °C, ranging from 1.13 °C in Jobos Bay, PR, to 4.91 °C in Delaware, DE. The average MHW mean intensity (Fig. 2c) was higher on the East Coast (3.40 °C) compared to the West Coast (2.53 °C). We note that changes in density associated with temperature increases observed during MHW events varied between 0.2 and 0.7 kg/m<sup>3</sup> and are therefore unlikely to impact stratification significantly

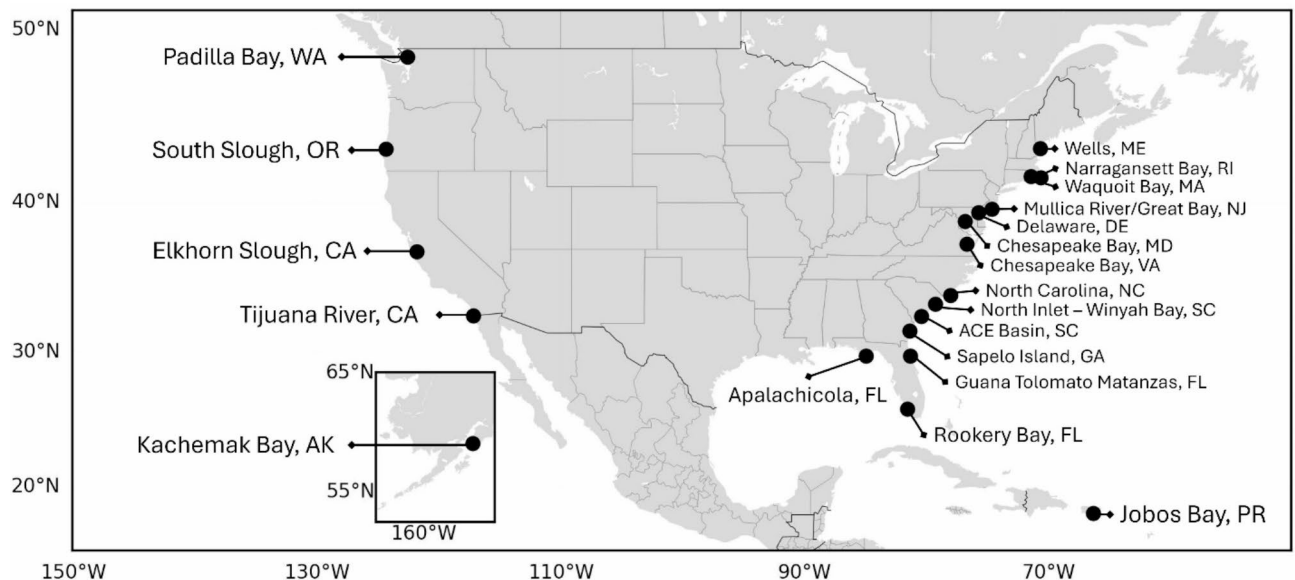


**Fig. 1.** Geographic distribution of National Estuarine Research Reserve System (NERRS) study sites across the United States. Map showing the locations of the 20 estuaries (reserves) included in the analysis of MHWs. Sites span both East and West coasts, as well as the Gulf of Mexico and Puerto Rico. Estuary names are labeled, and black dots indicate monitoring stations used for continuous temperature recordings over two decades.

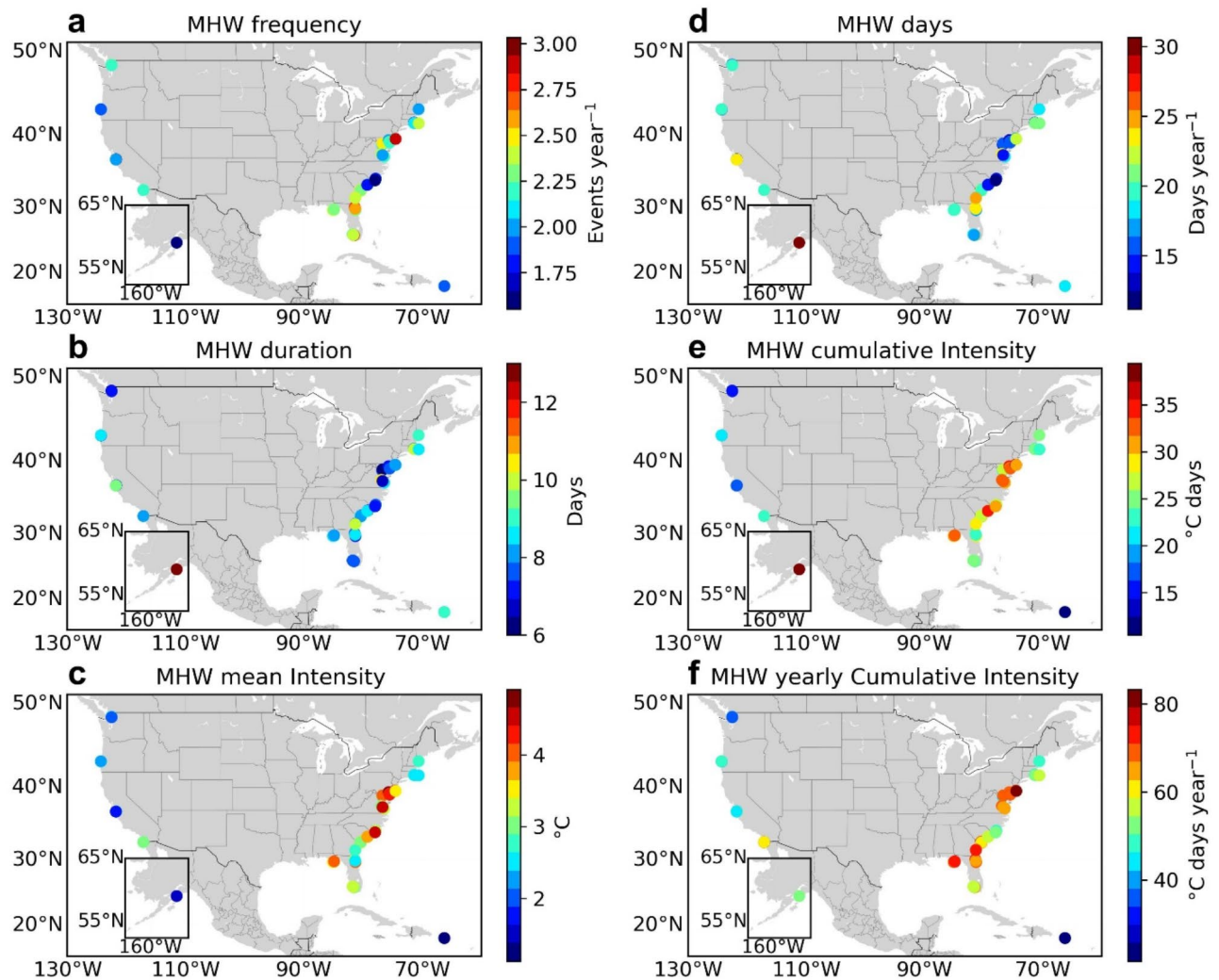


**Fig. 2.** Mean values of MHW metrics including **a** MHW frequency, **b** MHW duration, **c** MHW mean intensity, **d** MHW days, **e** MHW cumulative intensity, and **f** MHW yearly cumulative intensity, estimated from records over two decades-long (see Methods: Temperature dataset, Supplementary Table 2). Numeric values for these metrics are provided in Supplementary Table 3. The range of the colorbar for MHW duration was adjusted to better represent other locations, as the station in Kachemak Bay, AK, recorded a duration of 22.34 days.

compared to salinity-driven density variations, which often govern estuarine stratification, particularly in partially mixed and salt-wedge estuaries. Average MHW cumulative intensity (Fig. 2e) was higher on the East Coast (28.14 °C days) than on the West Coast (19.87 °C days), with an overall average of 26.14 °C days across all reserves. The weakest events occurred in Puerto Rico, PR (10.48 °C days), while the strongest were recorded at Kachemak Bay, AK (39.41 °C days). The average MHW yearly cumulative intensity (Fig. 2f) was 58.47 °C days per year across all reserves. The East Coast experienced more intense events (62.55 °C days per year) compared to the West Coast (48.92 °C days per year). Mean yearly cumulative intensity ranged from 21.53 °C days per year in Puerto Rico, PR, to 83.31 °C days per year in Mullica River/Great Bay, NJ. Additional detailed information on MHW metrics across all sites is provided in Supplementary Table 3.

### MHW co-occurrence

Distinct geographical patterns in the co-occurrence of MHW events were observed across regions, with notable influence of adjacent coastal areas (Fig. 3). On the East Coast, the Northeast (NE) region largely shared MHW events (~50% or greater co-occurrence) within its area and with some reserves in the Mid Atlantic (MA), though this relationship weakened farther south. It is worth noting that the stronger MHW co-occurrence observed within the Northeast, Mid-Atlantic, and Southeast regions is partly attributable to the closer geographic proximity of the NERES reserves within these regions. Similarly, stations within the MA had large co-occurrence values (~50% or greater), and shared MHW events with the northern part of the Southeast (SE) region, with decreasing values moving southward. Stations within the SE experienced substantial co-occurrence of MHW events, including those in parts of the MA and Gulf of Mexico (GM), but there was little to no overlap with

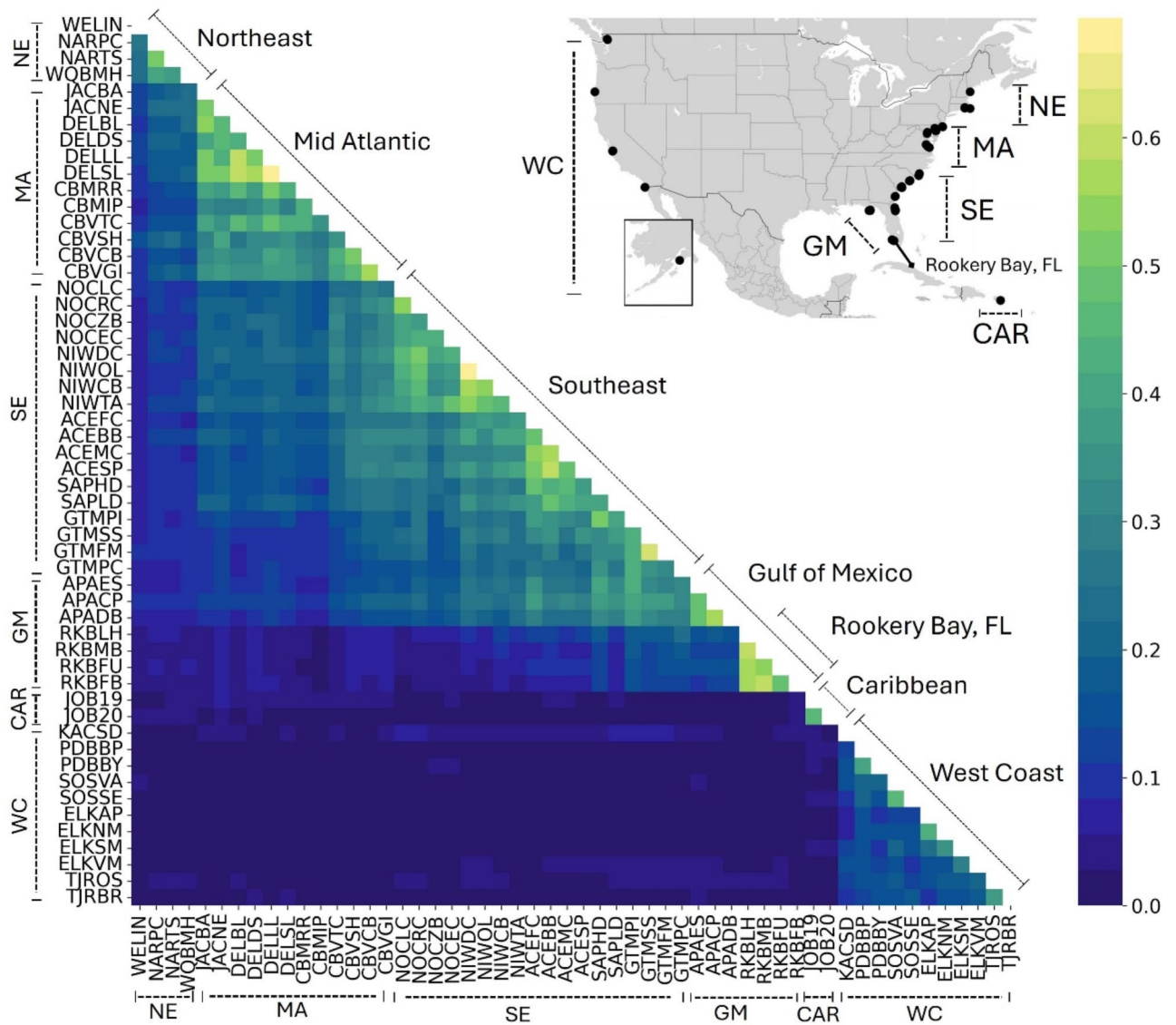


**Fig. 3.** Jaccard Index of MHWs across sites, with the top portion representing the northernmost sites and the bottom portion representing the southernmost sites, depicted from the East coast to the West coast. CAR represents Caribbean, GM stands for Gulf of Mexico, NE for Northeast, MA for Mid Atlantic, SE for Southeast, and WC for West Coast.

the NE. Rookery Bay (GM, Florida) experienced distinct MHW events, with limited co-occurrence primarily within its region and lower values with other stations within the GM. The Caribbean Reserve exhibited minimal co-occurrence, sharing MHW events only within its local area. On the West Coast, MHW events generally had moderate co-occurrence (~30–40%) across the entire coast, despite long distances between stations. Notably, little to no co-occurrence was observed with other regions. Alaska exhibited minimal co-occurrence, sharing MHW events only within its local area.

**MHW trends**

Over the past two decades, 30 out of 54 stations revealed statistically significant ( $p$ -value < 0.05) long-term increasing trends in MHWs (Fig. 4; Supplementary Table 4). Positive trends were predominantly observed on the East Coast, while most trends on the West Coast were not significantly different from zero at the 95% confidence level. Along the East Coast, MHW frequency (Fig. 4a) increased on average by 0.57 events per year per decade. In contrast, only two stations on the West Coast, located within Elkhorn Slough, CA and South Slough, OR had a statistically significant trend ( $p$ -value < 0.05) of 0.6 and 0.4 events per year per decade, respectively. MHW days (Fig. 4d) increased by an average of 11 days per decade across all East Coast sites. While the West Coast had no significant trends in MHW days ( $p$ -value > 0.05).

MHW yearly cumulative intensity (Fig. 4f) exhibited significant positive trends ( $p$ -value < 0.05) exclusively in East Coast reserves, with trends ranging from 20.12 to 53.39 °C days per year per decade (Delaware, DE and

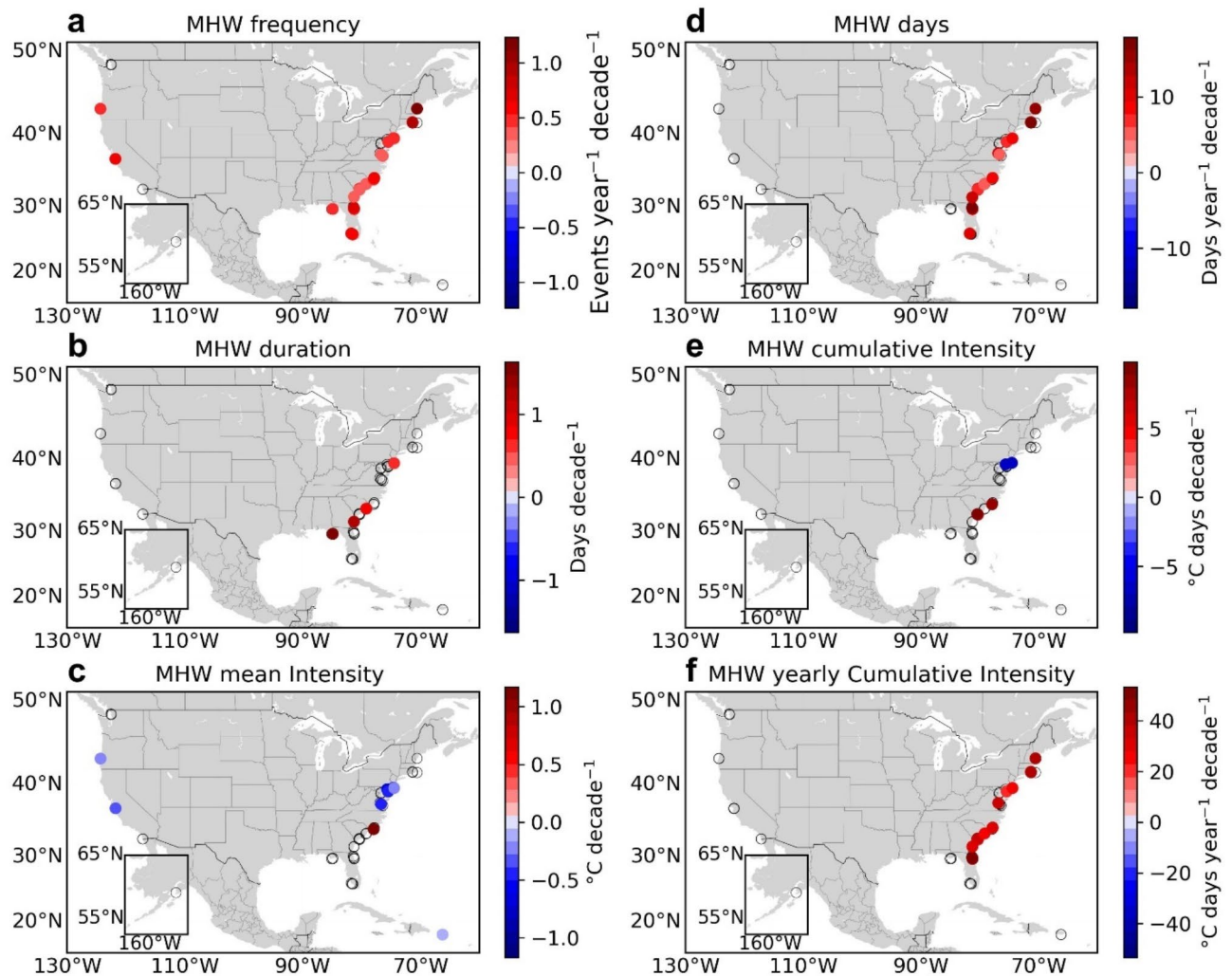


**Fig. 4.** Trends of MHWs metrics including: (a) MHW frequency, (b) MHW duration, (c) MHW mean intensity, (d) MHW days, (e) cumulative MHW intensity, and (f) MHW yearly cumulative intensity estimated from records over two decades-long (see Methods: Temperature dataset, Supplementary Table 2). Numeric values for these trends are provided in Supplementary Table 4. Empty circles indicate locations where trend estimates were not significantly different from zero (at the 95% confidence level).

ACE Basin, SC, respectively). On average, MHW yearly cumulative intensity in this region increased by over 37 °C days per year per decade. Trends in MHW mean intensity (Fig. 4c) were generally weak and negative, averaging  $-0.39$  °C per decade across nine out of 10 statistically significant ( $p$ -value  $< 0.05$ ) reserves on both coasts. Only one positive trend was observed, in North Carolina, NC, showing an increase of 1.17 °C per decade in MHW mean intensity. Relatively fewer significant trends ( $p$ -value  $< 0.05$ ) were observed in MHW cumulative intensity (Fig. 4e). Of the four East Coast stations, two were associated with positive trends of 9 °C days per decade, while the other two exhibited negative trends of  $-6$  °C days per decade. MHW duration (Fig. 4b) had significant trends ( $p$ -value  $< 0.05$ ) across four reserves on the East Coast, averaging 1.06 days per decade.

#### Impact of climate change and natural variability on MHW trends

The AR1 model (Eq. 2) parameters, fit, and the constant linear trends used to modify each time series are presented in Supplementary Fig. 1, 2; Tables 5 and 6. Results presented here represent classifications of statistically significant MHW trends at the 95% confidence level. On the East Coast, positive and stronger trends in MHW frequency, MHW days, and MHW yearly cumulative intensity (Fig. 5a, d, f) were largely driven by mean warming (Type 3), accounting for 40.7%, 47.4%, and 52.9% of the trends, respectively. While some stations attributed MHW trends solely to changes in SST variability (Type 2), these accounted for a much smaller fraction, contributing 11%, 10.5%, and 11.8%, respectively. The contribution to rising MHW trends attributed to both trends in mean SST and variability (Type 4), were more pronounced, accounting for 33%, 36.8%, and 29.4%. Stations where neither mean warming nor variability (Type 1) contributed to significant MHW trends accounted for 14.8% of MHW frequency, 5.3% of MHW days, and 5.9% of MHW yearly cumulative intensity.

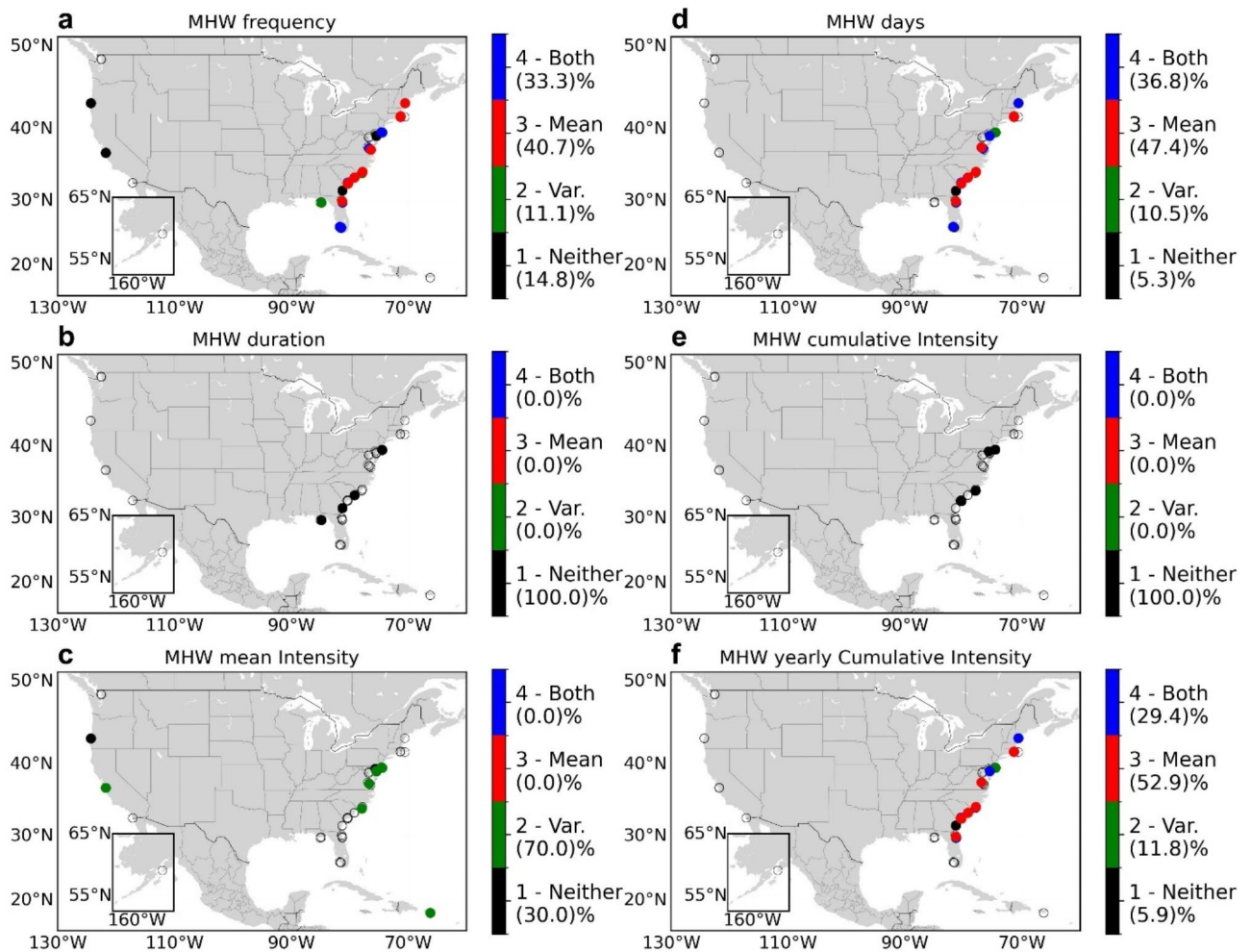


**Fig. 5.** The relative impact of changes in the mean and variability of SST on **a** MHW frequency, **b** MHW duration, **c** MHW mean intensity, **d** MHW days, **e** cumulative MHW intensity, and **f** MHW yearly cumulative intensity. The colors indicate whether trends in MHW metrics are dominated by trends in SST mean and/or variance. The four categories are shown as: neither in black, variance-dominated in green, mean-dominated in red, and both in blue. The percentage of all stations with significant trends dominated by each category is indicated in the colorbar. Classifications of trend attribution types for all stations are provided in Supplementary Table 6. Empty circles indicate locations where trend estimates were not significantly different from zero based on MHW trend analysis (at the 95% confidence level).

For MHW mean intensity (Fig. 5c), negative trends were observed in most stations, with 70% of these trends attributed solely to SST variability. The remaining 30% of significant trends could not be explained by either trends in mean warming or variability (Type 1). For MHW duration and cumulative intensity (Fig. 5b, e), all trends were classified as Type 1, indicating that they are not driven by changes in mean SST or variability.

### Climate modes of variability and MHW occurrences

Although eight indices were statistically correlated with SST anomalies ( $p$ -value < 0.05), as expected, some of the indices were substantially correlated to other indices (e.g. MEI, BEST, Niño 3.4) and produced similar results in MHW occurrences. To avoid redundancy, we present a subset of five key climate indices here (PDO, ONI, Niño 1 + 2, EP/NP, and NAO; Fig. 6) and include the remaining ones in the appendix (Supplementary Fig. 3). We found that the relationship between climate modes and SST anomalies was maximized at different time lags for each mode (Supplementary Table 7). Across all sites, the maximum correlation occurred at 1-month lag for PDO, a 3-month lag for ONI, a 5-month lag for Niño 1 + 2, a 1-month lag for EP/NP, and a 1-month lag for NAO. Accordingly, we report the relative percentage changes for the aforementioned lags.

Of these modes, the PDO had the greatest influence, with its positive phase leading to the highest increase in MHW occurrences exclusively along the West Coast (Fig. 6a). This ranged from 102.8% enhanced MHW occurrences at Elkhorn Slough, CA to 137.2% at Tijuana River, CA. In general, the positive PDO index was significant ( $p$ -value < 0.1) in five reserves across the West Coast. On average, the positive phase of the PDO increased MHW occurrences by 118.5%. On the other hand, East Coast reserves experienced an average decrease of 31.8% in MHW occurrences, with the positive PDO contributing to the reduction in seven reserves.

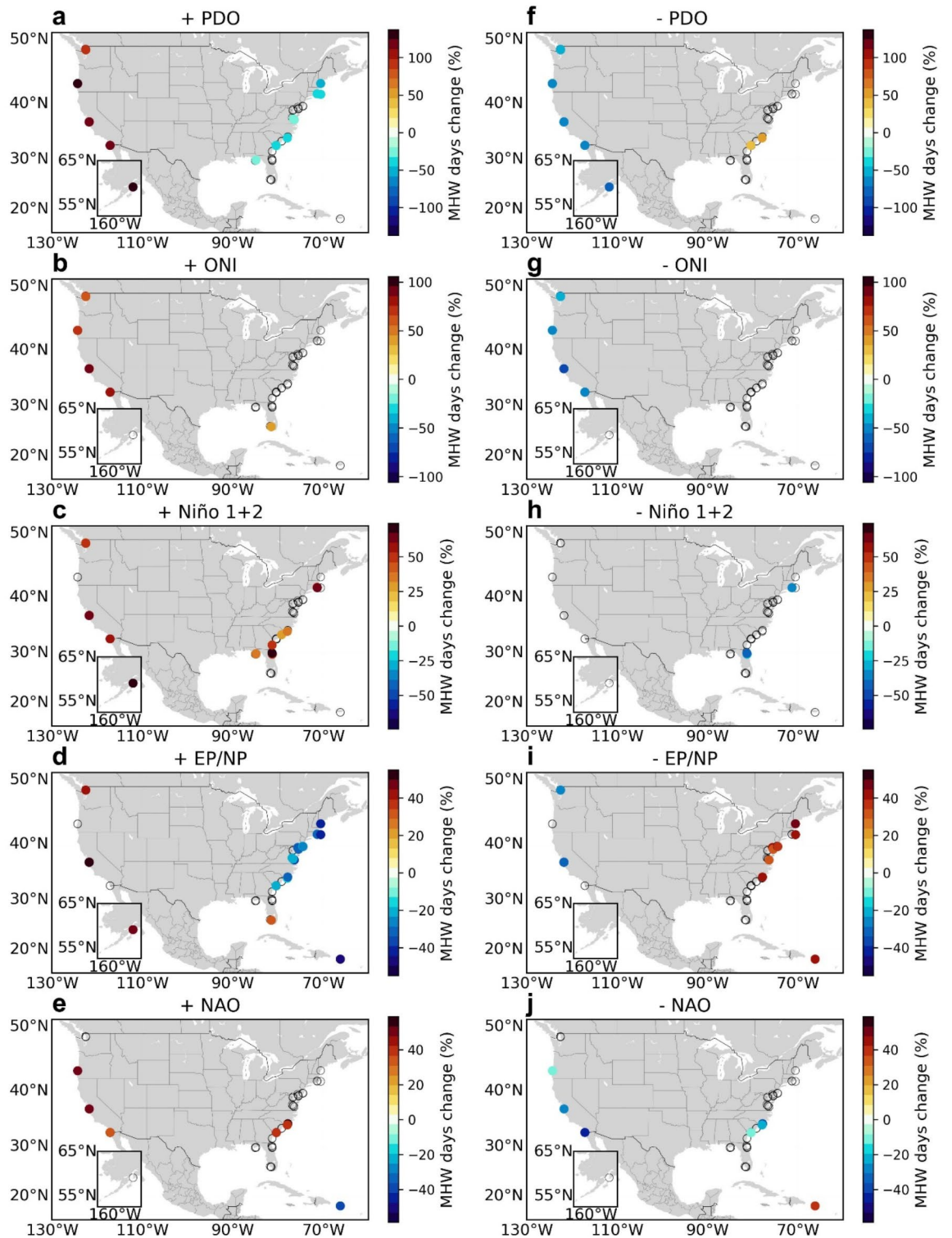


**Fig. 6.** The relative percent change in MHW occurrences during different phases of the **a, f** Pacific Decadal Oscillation (PDO) **b, g** Oceanic Niño Index (ONI) **c, h** Niño 1 + 2, **d, i** East Pacific/North Pacific Oscillation (EP/NP) and **e, j** North Atlantic Oscillation (NAO) at each location. Percent changes were calculated by subsetting the data into the phase of each respective climate mode and then comparing the number of MHW days to that of the original dataset. Numeric values of percentage changes are listed in supplementary Table 7. Empty circles indicate locations where the data was not statistically significant at the 95% confidence level.

The negative phase of PDO reduced MHW occurrences by an average of 65.7% (Fig. 6f), significantly impacting ( $p$ -value < 0.1) five reserves on the West Coast. Two reserves along the East Coast experienced an increase in MHW occurrences of up to 49.9% during the negative phase of the PDO.

The positive phase of the ONI (Fig. 6b) was associated with a significant increase in MHW occurrences in five reserves, mostly on the West Coast, with Rookery Bay, FL, being an exception in the Gulf of Mexico. On average, ONI increased MHW occurrences by 73.1%, with a weaker effect in the Gulf of Mexico (37.7%) and stronger effect in the Tijuana River, CA (105.7%). During its negative phase (Fig. 6g), ONI had a significant ( $p$ -value < 0.1) relationship with four reserves on the West Coast, where it reduced MHW occurrences by an average of 53.1%. With a magnitude and phase influence on MHW occurrences similar to ONI, Niño 3.4 (Supplementary Fig. 3c) had a broader geographic reach, significantly ( $p$ -value < 0.1) impacting reserves across both the East (eight reserves) and West Coasts (ten reserves).

Positive Niño 1 + 2 (Fig. 6c) had the second most extensive spatial influence, being associated with ten reserves across both the East and West Coasts and the Gulf of Mexico. On average, it increased MHW occurrences by 52.5%, ranging from 29.8% in North Inlet – Winyah Bay, SC, to 74.3% in Guana Tolomato Matanzas, FL. Negative Niño 1 + 2 (Fig. 6h) affected two reserves, exclusively on the East Coast, and reduced MHW occurrences by an average of 35.7%, with values ranging from –26.8% (Guana Tolomato Matanzas, FL) to –44.8% (Guana Tolomato Matanzas, FL).

The positive phase of the EP/NP (Fig. 6d) had the broadest spatial influence, affecting thirteen reserves across the East Coast (three reserves), West Coast (eight reserves), Puerto Rico (one reserve), and the Gulf of Mexico (one reserve). On average, it increased MHW occurrences by 45.3%, ranging from 33.8% in Rookery Bay, FL, to 55% in Elkhorn Slough, CA. However, on the East Coast, the positive phase of the EP/NP was associated with a mean reduction in MHW occurrences of 29.4%, ranging from –17% in Chesapeake Bay, VA, to –47.4% in Jobos Bay, PR. In contrast, the negative phase of the EP/NP (Fig. 6i) increased MHW occurrences on the East Coast by an average of 41.1%, influencing seven reserves, with values ranging from 32% in Delaware, DE, to 55.3% in Mullica River/Great Bay, NJ. Conversely, on the West Coast, the negative phase of the EP/NP had the opposite effect, decreasing MHW occurrences by an average of 29.7%.

The NAO had a weaker overall impact on MHW occurrences compared to the other indices previously discussed, with its positive phase increasing occurrences by an average of 45.6% (Fig. 6e), and its negative phase reducing occurrences by 24.7% (Fig. 6j). Across the East and West Coasts, the NAO was associated with changes in MHW occurrence at six reserves (three on the East Coast, two on the West Coast, and one in Puerto Rico). During the positive phase, the index increased occurrences from 33.8 to 58.8%, and during the negative phase, reduced MHW occurrences ranging from 10.5% (ACE Basin, SC) to 43.1% (Tijuana River, CA). Only Jobos Bay, PR, showed a 36.1% increase in MHW occurrences during the negative phase of the NAO and a 37.5% decrease during its positive phase.

## Discussion

### Climate change

Using a unique data set consisting of temperature measurements spanning more than two decades from 54 stations across 20 estuaries from the National Estuarine Research Reserve System in the US, we characterized long-term MHW trends and their relationship to climate change and variability. To the best of our knowledge, this is the most comprehensive assessment of estuarine MHWs and provides novel insights into the characteristics and trends of these extreme events in these ecologically and economically important environments.

Over the past two decades, there has been an increase in MHW frequency, MHW days per year, and yearly cumulative intensity (Fig. 4a, d, f), consistent with previous research that revealed similar trends in coastal areas worldwide<sup>22,36</sup>, and in the global ocean<sup>14,15</sup>. However, the trends in MHWs detected here were mostly concentrated on the U.S. East Coast, a region which also experiences higher-intensity events (mean, cumulative, and yearly cumulative intensities, Fig. 2c, e, f), and is therefore already more vulnerable to thermal stress in response to MHW events. If the observed increases in MHW days per year persist, MHWs in East Coast estuaries could potentially occur nearly a third of the year by the end of the century, with unprecedented ecosystem impacts. In contrast, trends in MHWs were only detected in two out of 10 stations along the U.S. West Coast (Fig. 4). Notably, trends in this region were highly sensitive to the Northeast Pacific heatwave<sup>50</sup>, a major multi-year event that occurred between 2014 and 2016. Excluding these years from our dataset resulted in no statistically significant trends at the 95% confidence level in any estuarine reserve along the U.S. West Coast.

In fact, studies along the U.S. West Coast and other Eastern Boundary Upwelling Systems (EBUS) have shown that long-term SST warming is less pronounced or even decreasing at some locations<sup>51–54</sup>, resulting in absence of trends in MHWs<sup>15,22,25,55</sup>. This is hypothesized to occur due to the persistent wind-driven upwelling along these regions, which brings colder water from depth to the surface. As a result, EBUS have responded differently to climate change compared to the rest of the globe and have been suggested to function as “thermal refugia” from global warming<sup>56–59</sup>. Our findings suggest that estuaries along the U.S. West coast, and potentially in other EBUS, are also influenced by the effects of upwelling, whether through advection of colder waters from the ocean to the estuary via exchange flow (e.g. MacCready & Geyer<sup>60</sup>), or by cold upwelled waters regulating local climate through air-sea interactions<sup>56,61,62</sup>, or both. We speculate that these estuaries could also serve as future “thermal refugia” in the face of global warming, potentially preserving their integrity during extreme events, as long as EBUS continue to buffer against warming induced by climate change (see Bograd et al.<sup>63</sup>).

Using a statistical climate model, we found that changes in the long-term mean SST are the dominant factor behind the increasing MHW frequency, MHW days per year, and MHW yearly cumulative intensity in nearly half of the U.S. estuaries with significant trends (Fig. 5a, d, f). These findings are consistent with previous results from global, coastal, and estuarine regions, despite differences in attribution methodologies<sup>15,16,21,22,49</sup>. On the other hand, SST variance was the dominant driver of MHW mean intensity, while neither change in mean nor

variance of SST fully explained trends in MHW duration and MHW cumulative intensity, making these metrics more challenging to project. Finally, our results suggest that continued warming of our planet over the next decades as projected by the Intergovernmental Panel on Climate Change<sup>64</sup> will lead to a further increase in MHW frequency, MHW days per year, and yearly cumulative intensity, especially in East Coast estuaries, where changes in mean SST dominate over changes in variance.

### Climate variability

We identified a strong link between the likelihood of estuarine MHW occurrence and large-scale climate modes of variability. Most estuaries along the U.S. West Coast experienced significant changes in MHW occurrences during different phases of PDO, ONI, Niño 1 + 2, EP/NP, and NAO (Fig. 6). Increases of as much as 137% in MHW occurrences were observed during the positive phase of the PDO, the climate index which had the greatest influence in estuaries studied here, modulating all of the estuarine reserves along the West Coast. During the positive phase of the ONI, increases of up to 105% were seen in estuarine reserves on the West Coast (not including Alaska). With lesser but still significant changes in the occurrences of MHWs, the positive phase of Niño 1 + 2 was associated with increases of MHW days of up to 74.3%, the positive phase of EP/NP was associated with increases of up to 55%, while the positive phase of NAO was associated with increases of up to 58.8%. The changes in likelihoods of MHW occurrences along the West Coast associated with the different climate indices analyzed here, suggests that in this region, MHWs are modulated by various temporal scales and are strongly influenced both by local changes in SST as well as remote forcings (see e.g., Dalsin et al.<sup>25</sup>). These factors, along with oceanic and atmospheric teleconnections that drive climatic fluctuations, can trigger regional air-sea heat fluxes and atmospheric feedback mechanisms, ultimately contributing to localized warming<sup>23,27,28,65–68</sup>.

Interestingly, most of the estuaries on the East Coast did not have a clear relationship with climate modes, except for eight reserves associated with EP/NP, six with PDO, five with Niño 1 + 2 and two reserves with the NAO. This suggests that key drivers of MHWs in this region may involve persistent local or remote forcings that are not strictly associated with large-scale climate modes, or internal variability resulting from short-term instabilities<sup>23,36,37</sup>. While a detailed dynamical analysis is beyond the scope of this study, our results suggest the need for further investigation into the primary drivers modulating MHW occurrences in East Coast estuaries at interannual time scales.

Overall, the magnitude of enhancement of MHW occurrences during positive phases of climate modes was greater than the suppression observed during the negative phases for all climate indices analyzed here. Individual climate modes contributed on average to a reduction in MHW occurrences during the negative phases ranging from nearly one- to two-thirds of the values observed during the positive phase. The only exceptions being the PDO and EP/NP indices, where both positive and negative phases led to both increases and decreases in MHW occurrences.

The relationship between MHW occurrences and climate modes is inherently complex<sup>23</sup>, and it becomes even more intricate in estuaries, due to additional influences from surrounding land/watersheds<sup>49</sup>. Nevertheless, the relationship between regionally enhanced or suppressed MHW occurrences and dominant climate modes has been well established for the global ocean<sup>23</sup>, and now similar links between these modes and MHW occurrences in estuaries have also been demonstrated here. Although we did not investigate the compounding effects of multiple large-scale climate modes, it is important to acknowledge that these modes can influence certain regions simultaneously due to their interdependencies<sup>23,25,69,70</sup>.

While statistical relationships do not prove causality, they often reveal important connections between climate indices and MHW occurrences that may suggest ways to predict future outcomes, potentially many months ahead<sup>23,28,30</sup>. The predictability of extreme events such as MHWs can be extremely helpful to marine resource users, as well as managers of fisheries, aquaculture and conservation efforts<sup>28,71–73</sup>. Early predictions of future MHWs from both short- and long-term forecasts could allow for proactive mitigation measures including, but not limited to, relocating endangered species, adjusting aquaculture operations, making strategic decisions in fisheries management (e.g., target species, quotas), or implementing protected areas to mitigate potential ecosystem and economic losses<sup>28</sup>. Further exploration of the underlying dynamical mechanisms is needed to enhance the predictability of these events.

### Regional contrasts

As previously discussed, there are notable differences in the modulation of MHW occurrences and their vulnerability to climate change between estuaries on the East and West coasts. Furthermore, MHW co-occurrence analysis conducted here (Fig. 3) highlights the strong relationship between stations within similar geographic regions (e.g. NE, MA, SE, etc.), providing evidence of coherent forcing spatial scales. Given the wide range of estuaries addressed here, covering different geomorphological, stratification, and circulation regimes<sup>74</sup>, as well as different spatial scales and residence times, the geographically similar co-occurrences strongly suggests that, to first order, atmospheric-estuary heat exchange is the dominant driver of MHWs in these systems (see also Mazzini and Pianca<sup>49</sup>). Future studies should carefully quantify all the terms in the heat budget, investigate what role different estuary characteristics play in dynamics of MHWs, and the connection between MHWs with the end members of estuarine system: rivers and the coastal ocean.

### Implications

Estuaries are highly productive yet vulnerable ecosystems that support a wide range of species, provide essential ecosystem services, and sustain vital economic activities. These environments serve as nurseries for over 75% of all fish and shellfish harvested in the US<sup>75</sup>, and support over 54 million jobs<sup>76</sup>. However, estuaries are exposed to diverse anthropogenic pressures (e.g., industrial pollution, eutrophication) and have been significantly threatened by climate change worldwide<sup>77–86</sup>. Moreover, many estuaries are currently facing major environmental

disturbances linked to MHW events, including fish kills<sup>41</sup>, deoxygenation and biodiversity loss<sup>42</sup>, long-lasting declines in macroalgae biomass<sup>43,44</sup>, shifts in seagrass dominance and carbon stocks<sup>45,46</sup>, low dissolved oxygen and pH levels<sup>47</sup>, and expansion of hypoxic zones<sup>48</sup>.

The continued human impact on estuarine ecosystems, compounded by extreme events like MHWs as temperatures rise throughout the twenty-first century, will lead to significant habitat loss and water quality degradation, causing long lasting and potentially permanent impacts to marine ecosystems. Future long-term climate change and subsequent increases in estuarine MHW frequency and intensity, particularly along the East Coast, could increase the vulnerability of estuarine habitats and threaten the ecosystem-services and economies they support<sup>4,5,13</sup>. This may require urgent ecosystem-based adaptation plans to mitigate the intensifying impacts and protect their resilience in a warming future.

## Methods

### Temperature dataset

High frequency in-situ water temperature measurements were obtained from the US National Oceanic and Atmosphere Administration's (NOAA) National Estuarine Research Reserve System (NERRS) for the period 1995 to 2023. NERRS is a network of 30 coastal sites that systematically monitors meteorological and water quality parameters across the United States. We analyzed near-surface water temperature data recorded at 15- and 30-minute intervals from sensors placed at depths of 0.3 to 4.5 m below the surface, except for the Kachemak (Alaska) reserve at 8.5 m, where the tidal range is considerably higher (~8.1 m). Temperature data flagged as being out of sensor range, rejected, or suspect during automated QAQC (Quality Assurance and Quality Control) processing developed for each respective site were excluded. Over the years, some stations were relocated by distances ranging from a few meters to up to 2 km, resulting in name changes. We merged data from five such stations to maintain consistent location representation and extend their record length (see Supplementary Table 1). To optimize spatial coverage while maintaining data integrity, we selected time series with a minimum record length of 20 years and less than 20% gaps, ensuring they remained robust for MHW analysis<sup>87</sup>. Out of 28 reserves (excluding Great Lakes sites) and 164 stations, a total of 54 stations from 20 estuarine reserves fulfilled these requirements and were selected for analysis (Fig. 1). Tidal and diurnal temperature variations were removed using a low-passed filter with a 40-hour cutoff, and then daily-averaged values were calculated. Gaps of up to 2 days were linearly interpolated. Detailed information about stations and data used in this research is presented in the Supplementary Table 2.

### Climate indices dataset

We considered nine commonly used climate indices linked to key modes of variability within the climate system and recognized for their influence on MHW occurrence in the Northern Pacific and Atlantic Ocean<sup>23,25</sup>. These modes vary on different time scales, ranging from seasonal (e.g., North Atlantic Oscillation - NAO) to longer (e.g., Pacific Decadal Oscillation - PDO). Indices were obtained from the NOAA Physical Sciences Laboratory (<https://psl.noaa.gov/data/climateindices/>). The specific climate indices included in our analysis were the NAO index, PDO index, Oceanic Niño (ONI) index, Niño 1+2 index, Niño 3.4 index, East Pacific/North Pacific Oscillation (EP/NP) index, Bivariate ENSO Timeseries (BEST) index, Multivariate ENSO (MEI) index, and Atlantic Multi-decadal Oscillation (AMO) index. All indices were originally available at monthly intervals and were subsequently linearly interpolated to daily values<sup>23</sup> by assigning monthly values to the first day of each month.

### MHW identification

We identified MHWs using the daily-averaged time series following Hobday et al.<sup>1</sup> and the Python module “marineHeatWaves” (available at <https://github.com/ecjolver/marineHeatwaves>). To establish a climatology, an 11-day moving-average window centered on the specific time of the year was used. The daily 90th percentile of the climatology was computed over the maximum time coverage of each dataset and was set as the threshold. MHWs were then identified when daily-averaged temperatures exceeded the daily threshold for five or more consecutive days, while allowing for a two-day drop below the threshold in between MHW events<sup>1</sup>. We examined MHW metrics including frequency, duration, mean intensity (mean deviation above the climatology), cumulative intensity, and yearly cumulative intensity, to evaluate their range and potential regional differences. To ensure better stability in the trend analysis of MHW yearly characteristics, we removed outliers using the Interquartile Range (IQR) method<sup>88</sup>. Long-term trends in the yearly averaged MHW characteristics were then assessed using linear regressions while trends in MHW yearly frequency were evaluated with a generalized linear model using a Poisson distribution and log link function.

### MHW co-occurrence

Co-occurrence of MHWs between different sites was calculated using the Jaccard index ( $J$ )<sup>89</sup>, which measures the similarity between two data sets. The Jaccard index is expressed as:

$$J(A, B) = \frac{|A \cap B|}{|A \cup B|} = \frac{|A \cap B|}{|A| + |B| - |A \cap B|} \quad (1)$$

where A and B represent the sets of MHW days recorded at two distinct locations. The index ranges from  $J=0$ , indicating no co-occurrence of MHW days, to  $J=1$ , indicating perfect overlap, where all MHW days in A occur in B and vice versa. Co-occurrence was calculated without applying time lags, as our analysis focused on MHW days occurring simultaneously at both locations.

### Trend attribution in MHW properties

We used a statistical climate model<sup>16</sup> to evaluate the contributions of climate change and natural variability in driving MHW trends. To do so, we simulated a daily SST time series with stationary statistical properties, using a first-order autoregressive (AR1) model:

$$T(t + \Delta t) = aT(t) + \epsilon(t) \quad (2)$$

where  $T(t)$  represents SST at time  $t$ ,  $\Delta t$  is the time step (1 day),  $a$  is the autoregressive parameter, and  $\epsilon(t)$  is a white noise process with zero mean and variance  $\sigma_\epsilon^2$ . We first removed the seasonal climatological mean and the linear trend from the observed SST. The AR1 model parameters were then estimated:  $a$  was computed through ordinary least squares regression of  $T_0$  lagged by 1 day, and  $\sigma_\epsilon$  was calculated as the standard deviation of the residuals. Next, we modified this time series by specifying either a constant linear trend in mean SST:

$$T_m = T + mt,$$

or in the SST variance:

$$T_v = T(1 + vt),$$

where  $T_m$  is the new time series with a linearly increasing mean but constant variance  $\sigma^2$ , and  $T_v$  is the series with linearly increasing variance but constant mean  $\mu$  (see Appendix in Oliver<sup>16</sup>). The constants  $m$  and  $v$  were derived from the observed trends in the deseasoned SST mean and variance. We then calculated MHWs for each modified time series. This process was repeated for  $N_e = 500$  independent realizations of  $\epsilon(t)$ , producing a set of MHWs trends, each reflecting a distinct realization of SST variability. Confidence intervals were established from the 2.5th and 97.5th percentiles of these distributions, with significance determined when the interval excluded zero<sup>16</sup>. These confidence intervals delineated the range of MHW trends expected solely from either change in the mean SST or in the SST variance. Finally, we classified each MHW metric into one of four distinct scenarios (see Fig. 3 in Oliver<sup>16</sup>):

- Type 1 (Neither): Trends in the MHW metric due to both SST mean and variance trends are not significantly different from zero.
- Type 2 (Variance-Dominated): Trends in the MHW metric due solely to SST variance trends are significant.
- Type 3 (Mean-Dominated): Trends in the MHW metric due solely to SST mean trends are significant.
- Type 4 (Both): Trends in the MHW metric due to both SST mean and variance trends are significant.

### MHW occurrence and climate modes of variability

Prior to assessing the relationship between climate modes and MHW occurrence, we calculated the cross-correlation between each linearly detrended climate index and the detrended sea surface temperature (SST) anomalies. Climate indices that did not correlate with the SST anomalies at the 95% confidence level were excluded from further analysis. Lag times were determined based on statistically significant mode correlation values across all anomaly datasets, considering periods of one year, thereby extending the influence of climate modes across all studied regions. For each time series, we then computed the relative percentage change in MHW days corresponding to the distinct phases of the climate indices. Following Holbrook et al.<sup>23</sup>, we first calculate the number of MHW days at each location and then classified the corresponding climate index into either a positive or negative phase. We compared the number of MHW days during each phase to those observed in the original dataset. To determine whether the observed number of MHW days significantly deviated from what could be expected by random chance, Monte Carlo simulations were employed. For each climate index, a synthetic time series was generated by preserving the original periodogram while randomizing the Fourier coefficient phases using uniform, independent distributions (e.g., Rudnick & Davis<sup>90</sup>). The number of MHW days during positive and negative phases of this synthetic index was then recalculated. This simulation process was repeated 10,000 times to produce a frequency distribution of the expected number of MHW days for each station and climate index. Confidence intervals were established based on the 5th and 95th percentiles of these distributions<sup>23</sup>.

### Data availability

We used only publicly available data. Values plotted in Figs. 2, 4 and 5 and 6 are provided in the Supplementary Material file. NOAA high-frequency, in situ, near-surface water temperature data were provided by the National Estuarine Research Reserve System (Centralized Data Management Office) from their website (<https://cdmo.barruch.sc.edu/>). Climate indices were obtained from the NOAA Physical Sciences Laboratory website (<https://psl.noaa.gov/data/climateindices/>).

Received: 13 November 2024; Accepted: 24 February 2025

Published online: 06 March 2025

### References

1. Hobday, A. J. et al. A hierarchical approach to defining marine heatwaves. *Prog. Oceanogr.* **141**, 227–238 (2016).
2. Pansch, C. et al. Heat waves and their significance for a temperate benthic community: A near-natural experimental approach. *Glob. Chang. Biol.* **24**, 4357–4367 (2018).
3. Oliver, E. C. J. et al. Projected marine heatwaves in the 21st century and the potential for ecological impact. *Front. Mar. Sci.* **6**, 734 (2019).

4. Smale, D. A. et al. Marine heatwaves threaten global biodiversity and the provision of ecosystem services. *Nat. Clim. Chang.* **9**, 306–312 (2019).
5. Smith, K. E. et al. Biological impacts of marine heatwaves. *Annu. Rev. Mar. Sci.* **15**, 119–145 (2023).
6. Marba, N. & Duarte, C. M. Mediterranean warming triggers seagrass (*Posidonia oceanica*) shoot mortality. *Glob. Chang. Biol.* **16**, 2366–2375 (2010).
7. Thomson, J. A. et al. Extreme temperatures, foundation species, and abrupt ecosystem change: An example from an iconic seagrass ecosystem. *Glob. Chang. Biol.* **21**, 1463–1474 (2015).
8. Wernberg, T. et al. An extreme Climatic event alters marine ecosystem structure in a global biodiversity hotspot. *Nat. Clim. Chang.* **3**, 78–82 (2013).
9. Chavez, F. P. et al. Biological and chemical consequences of the 1997–1998 El Niño in central California waters. *Prog. Oceanogr.* **54**, 205–232 (2002).
10. Whitney, F. A. Anomalous winter winds decrease 2014 transition zone productivity in the NE Pacific. *Geophys. Res. Lett.* **42**, 428–431 (2015).
11. Brown, B. E. & Suharsono Damage and recovery of coral reefs affected by El Niño related seawater warming in the thousand Islands, Indonesia. *Coral Reefs*. **8**, 163–170 (1990).
12. Edwards, M. S. Estimating scale-dependency in disturbance impacts: El Niños and giant Kelp forests in the Northeast Pacific. *Oecologia* **138**, 436–447 (2004).
13. Smith, K. E. et al. Socioeconomic impacts of marine heatwaves: Global issues and opportunities. *Science* **374**, 419 (2021).
14. Frölicher, T. L. & Fischer, E. M. Gruber, N. Marine heatwaves under global warming. *Nature* **560**, 360–364 (2018).
15. Oliver, E. C. J. et al. Longer and more frequent marine heatwaves over the past century. *Nat. Commun.* **9**, 1324 (2018).
16. Oliver, E. C. J. Mean warming not variability drives marine heatwaves trends. *Clim. Dyn.* **53**, 1653–1659 (2019).
17. Oliver, E. C. J. et al. Marine heatwaves. *Annu. Rev. Mar. Sci.* **13**, 313–342 (2021).
18. Plecha, S. M. & Soares, P. M. M. Global marine heatwave events using the new CMIP6 multi-model ensemble: From shortcomings in present climate to future projections. *Environ. Res. Lett.* **15**, 124058 (2020).
19. Frölicher, T. L. & Laufkötter, C. Emerging risks from marine heat waves. *Nat. Commun.* **9**, 2015–2018 (2018).
20. Laufkötter, C., Zscheischler, J. & Frölicher, T. L. High-impact marine heatwaves attributable to human-induced global warming. *Science* **369**, 1621–1625 (2020).
21. Xu, T. et al. An increase in marine heatwaves without significant changes in surface ocean temperature variability. *Nat. Commun.* **13**, 7396 (2022).
22. Marin, M., Feng, M., Phillips, H. E. & Bindoff, N. L. A global, multiproduct analysis of coastal marine heatwaves: Distribution, characteristics, and long-term trends. *J. Geophys. Res. Ocean* **126**, (2021). e2020JC016708.
23. Holbrook, N. J. et al. A global assessment of marine heatwaves and their drivers. *Nat. Commun.* **10**, 2624 (2019).
24. Oliver, E. C. J. et al. N. Marine heatwaves off Eastern Tasmania: Trends, interannual variability, and predictability. *Prog. Oceanogr.* **161**, 116–130 (2018).
25. Dalsin, M., Walter, R. K. & Mazzini, P. L. F. Effects of basin-scale climate modes and upwelling on nearshore marine heatwaves and cold spells in the California current. *Sci. Rep.* **13**, 12389 (2023).
26. Scannel, H. A., Pershing, A. J., Alexander, M. A., Thomas, A. C. & Mills, K. E. Frequency of marine heatwaves in the North Atlantic and North Pacific since 1950. *Geophys. Res. Lett.* **43**, 2069–2076 (2016).
27. Holbrook, N. J. et al. ENSO-driven ocean extremes and their ecosystem impacts. *El Niño South. Oscillat Chang. Clim.* 409–428 (2020).
28. Holbrook, N. J. et al. Keeping Pace with marine heatwaves. *Nat. Rev. Earth Environ.* **1**, 482–493 (2020).
29. Elzahaby, Y. & Schaeffer, A. Observational insight into the subsurface anomalies of marine heatwaves. *Front. Mar. Sci.* **6**, 745 (2019).
30. Jacox, M. G., Tommasi, D., Alexander, M. A., Hervieux, G. & Stock, C. A. Predicting the evolution of the 2014–2016 California current system marine heatwave from an ensemble of coupled global climate forecasts. *Front. Mar. Sci.* **6**, 497 (2019).
31. Amaya, D. J., Miller, A. J., Xie, S. P. & Kosaka, Y. Physical drivers of the summer 2019 North Pacific marine heatwave. *Nat. Commun.* **11**, 1–9 (2020).
32. Gupta, A. S. et al. Drivers and impacts of the most extreme marine heatwave events. *Sci. Rep.* **10**, 1–15 (2020).
33. Elzahaby, Y., Schaeffer, A., Roughan, M. & Delaux, S. Oceanic circulation drives the deepest and longest marine heatwaves in the east Australian current system. *Geophys. Res. Lett.* **48**, eGL094785 (2021). (2021).
34. Perez, E. et al. Understanding physical drivers of the 2015/16 marine heatwaves in the Northwest Atlantic. *Sci. Rep.* **11**, 1–11 (2021).
35. Schaeffer, A. & Roughan, M. Subsurface intensification of marine heatwaves off southeastern Australia: The role of stratification and local winds. *Geophys. Res. Lett.* **44**, 5025–5033 (2017).
36. Cook, F. et al. Marine heatwaves in shallow coastal ecosystems are coupled with the atmosphere: Insights from half a century of daily *in situ* temperature records. *Front. Clim.* **4**, 1012022 (2022).
37. Schlegel, R. W., Oliver, E. C. J., Perkins-Kirkpatrick, S., Kruger, A. & Smit, A. J. Predominant atmospheric and oceanic patterns during coastal marine heatwaves. *Front. Mar. Sci.* **4**, 323 (2017).
38. Schlegel, R. W., Oliver, E. C. J. & Chen, K. Drivers of marine heatwaves in the Northwest Atlantic: The role of air sea interaction during onset and decline. *Front. Mar. Sci.* **8**, 627970 (2021).
39. Scannell, H. A., Johnson, G. C., Thompson, L., Lyman, J. M. & Riser, S. C. Subsurface evolution and persistence of marine heatwaves in the Northeast Pacific. *Geophys. Res. Lett.* **47**, eGL090548 (2020). (2020).
40. Valle-Levinson, A. *Contemporary Issues in Estuarine Physics* (Cambridge University Press, 2010).
41. Alosairi, Y., Alsulaiman, N., Rashed, A. & Al-Houti, D. World record extreme sea surface temperatures in the Northwestern Arabian/Persian Gulf verified by *in situ* measurements. *Mar. Pollut Bull.* **161**, 111766 (2020).
42. Brauko, K. M. et al. Marine heatwaves, sewage and eutrophication combine to trigger deoxygenation and biodiversity loss: A SW Atlantic case study. *Front. Mar. Sci.* **7**, 590258 (2020).
43. Magel, C. L., Chan, F., Hessian-Lewis, M. & Hacker, S. D. Differential responses of eelgrass and macroalgae in Pacific Northwestestuaries following an unprecedented NE Pacific ocean marine heatwave. *Front. Mar. Sci.* **9**, 838967 (2022).
44. Marin Jarrin, M. J., Sutherland, D. A. & Helms, A. R. Water temperature variability in the Coos estuary and its potential link to eelgrass loss. *Front. Mar. Sci.* **9**, 930440 (2022).
45. Shields, E., Moore, K. & Parrish, D. Adaptations by *Zostera marina* dominated seagrass meadows in response to water quality and climate forcing. *Divers* **10**, 125 (2018).
46. Arias-Ortiz, A. et al. A marine heatwave drives massive losses from the world’s largest seagrass carbon stocks. *Nat. Clim. Change.* **8**, 338–344 (2018).
47. Tassone, S. J., Besterman, A. F., Buelo, C. D., Walter, J. A. & Pace, M. L. Co-occurrence of aquatic heatwaves with atmospheric heatwaves, low dissolved oxygen, and low pH events in estuarine ecosystems. *Estuar. Coast.* **45**, 707–720 (2022).
48. Shunk, N. P., Mazzini, P. L. F. & Walter, R. K. Impacts of marine heatwaves on subsurface temperatures and dissolved oxygen in the Chesapeake Bay. *J. Geophys. Res.* **129**, eJC020338 (2024). (2023).
49. Mazzini, P. L. F. & Pianca, C. Marine heatwaves in the Chesapeake Bay. *Front. Mar. Sci.* **8**, 750265 (2022).
50. Gentemann, C. L., Fewings, M. R. & García-Reyes, M. Satellite sea surface temperatures along the West Coast of the United States during the 2014–2016 Northeast Pacific marine heat wave. *Geophys. Res. Lett.* **44**, 312–319 (2017).

51. Varela, R., Lima, F. P., Seabra, R., Meneghesso, C. & Gómez-Gesteira, M. Coastal warming and wind-driven upwelling: A global analysis. *Sci. Total Environ.* **639**, 1501–1511 (2018).
52. Seabra, R. et al. Reduced nearshore warming associated with Eastern boundary upwelling systems. *Front. Mar. Sci.* **6**, 00104 (2019).
53. Santos, F., Gomez-Gesteira, M., deCastro, M. & Alvarez, I. Differences in coastal and oceanic SST trends due to the strengthening of coastal upwelling along the Benguela current system. *Cont. Shelf Res.* **34**, 79–86 (2012).
54. Santos, F., DeCastro, M., Gómez-Gesteira, M. & Alvarez, I. Differences in coastal and oceanic SST warming rates along the Canary upwelling ecosystem from 1982 to 2010. *Cont. Shelf Res.* **47**, 1–6 (2012).
55. Izquierdo, P., Taboada, F. G., González-Gil, R., Arrontes, J. & Rico, J. M. Alongshore upwelling modulates the intensity of marine heatwaves in a temperate coastal sea. *Sci. Total Environ.* **835**, 155478 (2022).
56. Bakun, A. et al. Anticipated effects of climate change on coastal upwelling ecosystems. *Curr. Clim. Change Rep.* **1**, 85–93 (2015).
57. Hu, Z. M. & Guillemin, M. L. Coastal upwelling areas as safe havens during climate warming. *J. Biogeogr.* **43**, 2513–2514 (2016).
58. Lourenço, C. R. et al. Upwelling areas as climate change refugia for the distribution and genetic diversity of a marine macroalga. *J. Biogeogr.* **43**, 1595–1607 (2016).
59. Garcia-Reyes, M. et al. Most Eastern boundary upwelling regions represent thermal refugia in the age of climate change. *Front. Mar. Sci.* **10**, 1158472 (2023).
60. MacCready, P., Geyer, W. & Rockwell Advances in estuarine physics. *Annu. Rev. Mar. Sci.* **2**, 35–58 (2010).
61. Large, W. G. & Danabasoglu, G. Attribution and impacts of upper-ocean biases in CCSM3. *J. Clim.* **19**, 2325–2346 (2006).
62. Curchitser, E., Small, J., Hedstrom, K. & Large, W. 3.7 Up- and downscaling effects of upwelling in the California current system, in Report of Working Group 20 on Evaluations of Climate Change Projections (Canada: North Pacific Marine Science Organization (PICES)), 98 (2011).
63. Bograd, S. J. et al. Climate change impacts on Eastern boundary upwelling systems. *Annu. Rev. Mar. Sci.* **15**, 303–328 (2023).
64. Lee, J. Y. et al. Future global climate: Scenario-based projections and near-term information. In *Climate Change 2021: The Physical Science Basis. Contribution of Working Group I To the Sixth Assessment Report of the Intergovernmental Panel on Climate Change* (ed. ed Masson-Delmotte, V.) 553–672 (Cambridge Univ. Press, (2021).
65. Ren, X. et al. The Pacific decadal Oscillation modulated marine heatwaves in the Northeast Pacific during past decades. *Commun. Earth Environ.* **4**, 218 (2023).
66. Sprintall, J. et al. ENSO oceanic teleconnections. *El Niño South. Oscillat Chang. Clim.* **337–359**, 15 (2020).
67. Taschetto, A. S. et al. ENSO atmospheric teleconnections. *El Niño South. Oscillat Chang. Clim.* **311–334**, 14 (2020).
68. Thompson, D. W. J. & Wallace, J. M. Regional climate impacts of the Northern hemisphere annular mode. *Science* **293**, 85–89 (2001).
69. Maher, N., Kay, J. E. & Capotondi, A. Modulation of ENSO teleconnections over North America by the Pacific decadal Oscillation. *Environ. Res. Lett.* **17**, 114005 (2022).
70. Capotondi, A., Sardeshmukh, P. D., Di Lorenzo, E., Subramanian, A. C. & Miller, A. J. Predictability of US West Coast ocean temperatures is not solely due to ENSO. *Sci. Rep.* **9**, 10993 (2019).
71. Salinger, M. J. et al. The unprecedented coupled ocean-atmosphere summer heatwave in the new Zealand region 2017/18: Drivers, mechanisms and impacts. *Environ. Res. Lett.* **14**, 044023 (2019).
72. Dunstan, P. K. et al. How can climate predictions improve sustainability of coastal fisheries in Pacific Small- Island developing States? *Mar. Policy.* **88**, 295–302 (2018).
73. Smith, G. & Spillman, C. New high-resolution sea surface temperature forecasts for coral reef management on the great barrier reef. *Coral Reefs.* **38**, 1039–1056 (2019).
74. Valle-Levinson, A. *Introduction To Estuarine Hydrodynamics* (Cambridge University Press, 2022).
75. Office for Coastal Management National Estuarine Research Reserves. What is an estuary? An ecosystem, comprising both the biological and physical environment. *National Ocean. Atmospheric Administration* <https://coast.noaa.gov/nerrs/about/what-is-a-n-estuary.html> (accessed 20 Sep 2024).
76. Rouleau, T. et al. The Economic Value of America's Estuaries: 2021 Report. *Publications.2* (2021).
77. Ashizawa, D. & Cole, J. J. Long-term temperature trends of the Hudson river: A study of the historical data. *Estuaries* **17**, 166–171 (1994).
78. Najjar, R. G. et al. Potential climate-change impacts on the Chesapeake Bay. *Estuar. Coast Shelf Sci.* **86**, 1–20 (2010).
79. Seekell, D. A. & Pace, M. L. Climate change drives warming in the Hudson river estuary, new York (usa). *J. Environ. Monit.* **13**, 2321–2327 (2011).
80. Ding, H., Elmore, A. J. & Bay Spatio-temporal patterns in water surface temperature from landsat time series data in the chesapeake *U S Remote Sens. Environ* **168**, 335–348 (2015).
81. Oczkowski, A. et al. Preliminary evidence for the amplification of global warming in shallow, intertidal estuarine waters. *PLoS ONE.* **10**, e0141529 (2015).
82. Hinson, K., Friedrichs, M. A. M., St-Laurent, P., Da, F. & Najjar, R. G. Extent and causes of Chesapeake Bay warming. *J. Am. Water Resour. Assoc.* **58**, 805–825 (2022).
83. Bashevkin, S. M., Mahardja, B. & Brown, L. R. Warming in the upper San Francisco estuary: Patterns of water temperature change from five decades of data. *Limnol. Oceanogr.* **67**, 1065–1080 (2022).
84. Scanes, E., Scanes, P. R. & Ross, P. M. Climate change rapidly warms and acidifies Australian estuaries. *Nat. Commun.* **11**, 1803 (2020).
85. Shi, J. & Hu, C. South Florida estuaries are warming faster than global oceans. *Environ. Res. Lett.* **18**, 014003 (2023).
86. Prum, P., Harris, L. & Gardner, J. Widespread warming of Earth's estuaries. *Limnol. Oceanogr. Lett.* **9**, 268–275 (2024).
87. Schlegel, R. W., Oliver, E. C., Hobday, A. J. & Smit, A. J. Detecting marine heatwaves with sub-optimal data. *Front. Mar. Sci.* **6**, 737 (2019).
88. Dekking, F., Kraaikamp, C., Lopuhaa, H. & Meester, L. *A Modern Introduction To Probability and Statistics: Understanding why and How* (Springer, 2005).
89. Jaccard, P. Distribution de La Flore alpine Dans Le Bassin des Dranses et Dans Quelques Rgions Voisines. *Bull Soc. Vaudoise Des. Sci Nat.* **37**, 241–272 (1901).
90. Rudnick, D. L. & Davis, R. E. Red noise and regime shifts. *Deep Sea Res. I Oceanogr. Res. Pap.* **50**, 691–699 (2003).

## Acknowledgements

We sincerely thank Carl Friedrichs, Jian Shen, and Eric Hilton for their insightful discussions and valuable contributions. We also appreciate the editor and two anonymous reviewers for their constructive feedback, which greatly improved and shaped this work. We also acknowledge the essential contributions of the NERRS personnel, whose dedication and effort in maintaining consistent, reliable monitoring data made this research possible.

## Author contributions

R.U.N. performed the analysis and wrote the original draft of the paper; R.U.N., P.L.F.M. and R.K.W. contributed to the initial design and concept of the study. All authors (R.U.N., P.L.F.M., and R.K.W.) participated in result

discussions, assisted with interpretation, and contributed to writing the paper.

## Declarations

### Competing interests

The authors declare no competing interests.

### Additional information

**Supplementary Information** The online version contains supplementary material available at <https://doi.org/10.1038/s41598-025-91864-6>.

**Correspondence** and requests for materials should be addressed to R.U.N.

**Reprints and permissions information** is available at [www.nature.com/reprints](http://www.nature.com/reprints).

**Publisher's note** Springer Nature remains neutral with regard to jurisdictional claims in published maps and institutional affiliations.

**Open Access** This article is licensed under a Creative Commons Attribution-NonCommercial-NoDerivatives 4.0 International License, which permits any non-commercial use, sharing, distribution and reproduction in any medium or format, as long as you give appropriate credit to the original author(s) and the source, provide a link to the Creative Commons licence, and indicate if you modified the licensed material. You do not have permission under this licence to share adapted material derived from this article or parts of it. The images or other third party material in this article are included in the article's Creative Commons licence, unless indicated otherwise in a credit line to the material. If material is not included in the article's Creative Commons licence and your intended use is not permitted by statutory regulation or exceeds the permitted use, you will need to obtain permission directly from the copyright holder. To view a copy of this licence, visit <http://creativecommons.org/licenses/by-nc-nd/4.0/>.

© The Author(s) 2025